Passivation Mechanism of the High-performance Titanium Oxide Carrier-selective Contacts on Crystalline Silicon Studied by Spectroscopic Ellipsometry

Kazuhiro Gotoh[1]*, Hiroyuki Miura[1], Ayako Shimizu[1], Yasuyoshi Kurokawa[1] and Noritaka Usami[1]*

[1]*Department of Materials Process Engineering, Graduate School of Engineering, Nagoya University, Furo-cho, Chikusa-ku, Aichi 464-8603, Japan*

E-mail: gotoh.kazuhiro@material.nagoya-u.ac.jp, usa@material.nagoya-u.ac.jp

Variable-angle spectroscopic ellipsometry (SE) analysis is performed to study the impact of post-deposition annealing on the passivation performance of the heterocontacts consisting of titanium oxide and silicon oxide on crystalline silicon (c-Si) prepared by atomic layer deposition (ALD) for development of the high performance ALD-TiO_x/SiO_y/c-Si heterocontacts. The highest lifetime of 1.8 ms is obtained for the TiO_x/SiO_y/c-Si heterocontacts grown at 175 °C after annealing at 275 °C for 3 min. With increasing annealing temperature, the TiO_x layers of the TiO_x/SiO_y/c-Si heterocontacts become dominant. Furthermore, the amplitude of dielectric functions of the ALD-TiO_x layer decreases as annealing temperature increases, which suggests that enhanced diffusion of Ti into SiO_y interlayers at higher annealing temperature. The sufficient diffusion of Ti atoms into SiO_y interlayers is caused by annealing at 275 °C for 3 min, yielding high quality interface passivation.

1. Introduction

Passivation of crystalline silicon (c-Si) surface is crucial technique to achieve high performance silicon heterojunction (SHJ) solar cells.[1-3] SHJ solar cells exhibit high power conversion efficiency by using the stacks of intrinsic and doped hydrogenated amorphous silicon (a-Si:H).[4,5] The intrinsic a-Si:H (i-a-Si:H) is of importance for the conventional SHJ solar cells due to its excellent passivation effect. The i-a-Si:H passivating contacts reduces defects at a-Si:H/c-Si heterointerfaces, which leads to high open-circuit voltage.[6,7] Recently, titanium oxides (TiO_x) prepared by atomic layer deposition (ALD) attracts much attention as a novel carrier-selective contact, since the ALD-TiO_x provides high effective carrier lifetime (τ_{eff}), often used as quantitative figure of merit for passivation performance, after post deposition annealing.[8-17] Indeed, Yang *et al*. demonstrated high power conversion efficiency by the SHJ solar cells using ALD-TiO_x heterocontacts.[18]

So far, we have developed the ALD-TiO_x/SiO_y/c-Si heterocontacts for use in SHJ solar cells and thus obtained the high τ_{eff} of 1.4 ms after forming gas annealing (FGA).[17] Furthermore, the passivation mechanism of ALD-TiO_x/SiO_y/c-Si was investigated by combining high resolution transmission electron microscope and electron energy loss spectroscopy and hence we concluded that diffusion of Ti and O atoms into the SiO_y interlayer cause the enhancement of passivation performance.[17] Recently, the high τ_{eff} of 1.7 ms has been demonstrated after FGA by employing the SiO_y interlayer prepared by mixture of hydrochloric acid, hydrogen peroxide and deionized water, often called standard clean 2 (SC2).[19] Awaji *et al*. reported that the SiO_y layer prepared by the SC2 solution is the lowest film density.[20,21] Therefore, we considered that the highest passivation is caused by the enhanced diffusion of Ti atoms around the TiO_x/SiO_y heterointerfaces owing to the SiO_y interlayer with low density. Although comprehension of passivation mechanism of the ALD-TiO_x/SiO_y/c-Si heterocontacts is significantly important for further sophistication of SHJ solar cells, the diffusion of Ti is not fully unveiled.

Variable-angle spectroscopic ellipsometry (SE) is a powerful tool to determine layer thickness and optical constant of ultrathin films.[22,23] The SE exhibits extreme sensitvity of layer thickness with Angstrom order.[24] Furthermore, The dielectric function of materials and its structural properties strongly correlate with each other, meaning the structural properties can be predicted by the dielectric function. Direct observation of local structure in atomic scale is possible by transmission electron microscope, however large quantity of samples cannot be performed in a limited time. X-ray spectroscopy is sensitive to surface and thus the effect of surface contamination against ultrathin films is not neglected. Since the

layer thickness and optical constant of very thin films can be nondestructively and instantly investigated by SE, we address the local diffusion at the TiO_x/SiO_y heterointerfaces by using SE.

In this article, we studied the change in layer thickness and optical constant of the ALD-TiO_x/SiO_y/c-Si heterocontacts by variable-angle SE so as to investigate diffusion of Ti atoms into the SiO_y interlayers after FGA. Although part of this paper is presented in in SSDM2020[25], we expanded the range of growth temperature and analysis is dielectric function is included to discuss the diffusion of Ti atoms into the SiO_y interlayers.

2. Experimental methods

Floating zone grown, double side mirror-polished c-Si(100) wafers were used as substrates. The wafer thickness and resistivity were 280 ± 20 μm and 2-4 Ω·cm, respectively. Prior to depositing the ALD-TiO_x, the c-Si substrates were cleaned by 5% hydrofluoric acid to strip off the native oxide on the c-Si substrates. Following the c-Si substrates were rinsed in deionized water (DIW), they were dipped into SC2 solutions (hydrochloric acid/hydrogen peroxide/deionized water = 1:1:6) for 10 min to form ultrathin SiO_y layers. The substrates were loaded in ALD chamber after rinse in DIW. The ~3-nm-thick TiO_x layer was deposited on both sides of the c-Si substrates by ALD (GEMStar-6, Arradiance Inc.). In the ALD process, the titanium precursor, oxidizer and purge gas were tetrakis-dimethyl-amido titanium (TDMAT), H_2O and N_2 (99.9995%), respectively. The bottle for TDMAT was heated at 60 °C during ALD process. The deposition temperatures (T_{depo}) were 125, 150, 175, 200 and 225 °C. After depositing the TiO_x, FGA was carried out in the mixture gas of 97% Ar and 3% H_2 in order to improve passivation effect. The annealing temperature (T_{anneal}) was varied from 150 to 350 °C and the annealing duration was fixed at 3 min.

The injection-dependent τ_{eff} of the TiO_x/SiO_y/c-Si heterocontacts before and after FGA was measured by WCT-120TS lifetime tester (Sinton Instrument) at room temperature to investigate surface passivation performance.[26,27] The layer thickness and TiO_x dielectric function $\varepsilon_{TiOx}(E) = \varepsilon_1(E) - i\varepsilon_2(E)$ were characterized by variable angle SE (M-2000DI, J. A. Woollam). In all SE measurements, the amplitude ratio (ψ) and phase difference (Δ) spectra were acquired at three different incident angles of 65, 70 and 75°. To model dielectric functions of the ALD-TiO_x layer, Tauc-Lorentz model was employed. The Tauc-Lorentz model is widely applied to amorphous materials and the $\varepsilon_2(E)$ of the Tauc-Lorentz model is expressed by the product of Lorentz model and Tauc gap as follows,

$$\varepsilon_2(E) = \begin{cases} \dfrac{ACE_0\left(E - E_g\right)^2}{(E^2 - E_0^2)^2 + C^2E^2}\dfrac{1}{E} & \left(E > E_g\right), \\ 0 & \left(E \le E_g\right), \end{cases} \quad (1)$$

where, A, C, E_0, and E_g are the amplitude parameter, broadening parameter, peak transition energy, and Tauc optical gap, respectively.[28,29] The $\varepsilon_1(E)$ of the Tauc-Lorentz model is obtained by using Kramers-Kronig relations and is given by

$$\varepsilon_1(E) = \varepsilon_1(\infty) + \frac{2}{\pi}P\int_{E_g}^{\infty}\frac{\xi\varepsilon_2(\xi)}{\xi^2 - E^2}d\xi, \quad (2)$$

where the P represents the Cauchy principal part of the integral and $\varepsilon_1(\infty)$ is the energy-independent parameter at high energy.[28,29] The analytical solution of Eq. (2) is given elsewhere.[28,29] For the SiO_y interlayers, the optical constant was determined by Sellmeier model.[30] The optical constant of the SiO_y interlayers was determined by analyzing single SiO_y layer on c-Si substrate and was fixed for analyses on the TiO_x/SiO_y/c-Si heterocontacts. Thereby, seven parameters $\{A, C, E_0, E_g, \varepsilon_1(\infty), t_{TiOx}, t_{SiOy}\}$ were fitted in SE analyses and thus ε_{TiOx} (E) were derived, where t_{TiOx} and t_{SiOy} represent layer thickness of the ALD-TiO_x layers and the SiO_y interlayers, respectively. The schematic optical model is illustrated in Figure 1.

3. Results and discussion

Figure 2 (a) shows the τ_{eff} of the TiO_x/SiO_y/c-Si heterocontacts grown at 125, 175 and 225 °C as a function of minority carrier density (MCD). The τ_{eff} are improved after FGA at 275 °C for 3 min. Figure 2 (b) and (c) shows the impact of T_{anneal} and T_{depo} on τ_{eff} of the TiO_x/SiO_y/c-Si heterocontacts at MCD of 1×10^{15} cm^{-3}, respectively. The τ_{eff} tends to increase with increasing T_{anneal} from 150 to 275 °C, while the decrease in the τ_{eff} set in T_{anneal} = 320 °C. From Fig. 2 (c), the τ_{eff} increased with increasing T_{depo} upto 175 °C and decreased at T_{depo} from 200 °C. The highest lifetime of 1.8 ms was obtained for the TiO_x/SiO_y/c-Si heterocontacts grown at 175 °C after FGA at 275 °C for 3 min. It is stated that Ti diffusion into the SiO_y interlayers is a key to improve the passivation performance.[17] To investigate the Ti diffusion, variation of layer thickness and dielectric functions were characterized by SE analyses.

Figure 3 shows amplitude ratio (ψ) and phase difference (Δ) spectra of the TiO_x/SiO_y/c-Si heterocontacts fabricated at T_{depo} = 175 °C (a) before and (b) after annealing at 275 °C for 3 min. The mean square error (MSE) values of all SE analyses were ranged in 1.2-1.8, indicating the optical model was reasonable. Reiners *et al*. reported that T_{depo}

lower than 200 °C leads to quasi-amorphous films.[31] Furthermore, we previously reported that the TiO_x is amorphous after FGA.[17] These results suggest the ALD-TiO_x layers are amorphous before and after FGA. A good fitting to experimental data is obtained by using the optical model, indicating dielectric function modeling of the TiO_x/SiO_y/c-Si heterocontacts can be performed.

Figure 4 shows (a) total layer thickness of the TiO_x/SiO_y/c-Si heterocontacts (t_{total}), (b) ratio of t_{TiOx} to t_{total} and (c) t_{SiOy} to t_{total}. Compared with the as-deposited samples, t_{total} and t_{SiOy}/t_{total} increased after annealing at 150 °C, while t_{TiOx}/t_{total} decreased. This implies enhanced oxidation around SiO_y/c-Si interfaces. With increasing T_{anneal}, t_{total} gradually decreased possibly due to densification of the TiO_x/SiO_y heterocontacts. We reported that the TiO_x/SiO_y heterocontacts could be densified after annealing.[17] Furthermore, t_{TiOx}/t_{total} increased, whereas the t_{SiOy}/t_{total} decreased as T_{anneal} increased, indicating that the TiO_x layers in the TiO_x/SiO_y/c-Si heterostructures became dominant. Note that the optical constant of the SiO_y interlayer was fixed in SE analyses and thus structural property of pristine SiO_y interlayer was maintained except for t_{SiOy}. Thereby, the decreased t_{SiOy}/t_{total} denotes reduction of the pristine SiO_y interlayer. These behaviors suggest that diffusion of Ti atoms into SiO_y layers is induced by FGA and is enhanced at higher T_{anneal}.

In addition, smaller t_{total} was observed for the samples prepared at higher T_{depo}, which suggests ALD-TiO_x became compact by employing higher T_{depo}. As T_{depo} was elevated, t_{TiOx}/t_{total} and t_{SiOy}/t_{total} tends to be larger and smaller, respectively. As mentioned above, this can be explained by enhanced Ti diffusion during the growth of the TiO_x. At higher T_{depo}, indiffusion of the Ti atoms into the SiO_y interlayer would be enhanced and thus larger t_{TiOx}/t_{total} and smaller t_{SiOy}/t_{total} were obtained. The details about diffusion of Ti atoms is discussed later by correlating with dielectric functions.

Figure 5 shows the real and imaginary parts of the dielectric functions of the ALD-TiO_x layers prepared at T_{depo} = (a) 125, (b) 175, and (c) 225 °C. For as-deposited samples, the peak amplitude of ε_1 and ε_2 spectra are 9.81 and 6.76 for (a), 8.98 and 6.18 for (b), 8.92 and 6.12 for (c), respectively. After annealing up to 350 °C, the peak amplitude of $\varepsilon_1(E)$ and $\varepsilon_2(E)$ were reduced to about 8.84 and 5.91 for (a), 8.52 and 5.68 for (b), 8.41 and 5.66 for (c), respectively. The peak amplitude of $\varepsilon_1(E)$ and $\varepsilon_2(E)$ shows tendency to decrease as T_{depo} and T_{anneal} increased. The reduced $\varepsilon_1(E)$ and $\varepsilon_2(E)$ can be explained by crystallization of ALD-TiO_x, lowering density of ALD-TiO_x layer, formation of mixed TiO_x with SiO_y. Figure 6 shows refractive index n of the TiO_x layers at a wavelength of 500 nm as function of T_{depo} and T_{anneal}. The n values were computed from $\varepsilon_1(E) = n(E)^2 - k(E)^2$ and $\varepsilon_2(E)$ =

$2n(E)k(E)$, where $n(E)$ and $k(E)$ are refractive index and extinction coefficient, respectively. Figure about k is not shown here, since computed k values at 500 nm are zero. Larger n values were obtained at lower T_{depo} and T_{anneal}, and n tended to be smaller at higher T_{depo} and T_{anneal}. It is reported by Mardare and Hones that increase in refractive index and decrease in extinction coefficient of sputtered TiO_2 thin films are observed by transition from amorphous to crystalline phase.[32] Furthermore, Amor *et al*., reported that increasing n and decreasing k at 500 nm are observed for sputtered titanium oxide films with annealing temperature owing to improved compactness of the TiO_x films.[33] Since the decreasing trend of n was observed for the TiO_x/SiO_y/c-Si heterocontacts with increasing T_{depo} and T_{anneal}, crystallization and densification of the ALD-TiO_x is less effective on the dielectric function after annealing. Note that compactness of the TiO_x/SiO_y heterostructures would be enhanced at higher T_{depo} and T_{anneal}, since the decrease in t_{total} with increasing T_{depo} and T_{anneal} is observed in Figure 4. Further, the refractive index of SiO_2 is smaller than that of TiO_x,[30,32] and thus Si incorporated TiO_x probably exhibits small dielectric function compared with the original TiO_x. Hence, we consider that decrease in optical constant is attributed to intermixing of Ti and Si at the TiO_x/SiO_y heterointerfaces after annealing. It is noted again that the heterocontacts are modeled as the stacks of TiO_x and SiO_y without mixing layer into consideration, and the optical constant of the SiO_y interlayer was maintained in SE analyses. From Fig. 3, the increase in t_{TiOy}/t_{total} and decrease in t_{SiOy}/t_{total} are observed after annealing. In addition, decreasing trend of optical constant of TiO_x layer is observed. These results suggest that Si incorporated TiO_x become dominant and pristine SiO_y interlayer is reduced with increasing T_{anneal}.

From these results, we concluded that Ti diffusion is responsible for the passivation performance of the TiO_x/SiO_y/c-Si heterocontacts. The improved τ_{eff} is caused by the enhanced diffusion of Ti atoms and formation to the mixed oxide consisting of Si, Ti, O atoms. The degradation of the passivation performance can be explained by excessive diffusion of Ti atoms near the c-Si surface. It is well known that metal contaminations on c-Si surface damage severely electrical properties of Si based devices.[34-36] Thus, the highest τ_{eff} was obtained at T_{depo} = 175 °C and T_{anneal} = 275 °C.

4. Conclusions

We studied the effect of post-deposition annealing on the ALD-TiO_x/SiO_y/c-Si heterocontacts by using variable-angle spectroscopic ellipsometry. For SE analyses, we employed Tauc-Lorentz model to express dielectric function of for the ALD-TiO_x layers.

Low MSE values ranged in 1.2-1.8 are obtained for all SE analyses, indicating the dielectric functions of the 3-nm-thick ALD-TiO_x layers can be expressed by Tauc-Lorentz model at annealing temperature upto 350 °C. From injection-dependent τ_{eff} measurements, the τ_{eff} tends to increase with increasing T_{anneal} up to 275 °C and decreased from T_{anneal} = 320 °C. The highest lifetime of 1.8 ms was obtained for the TiO_x/SiO_y/c-Si heterocontacts grown at 175 °C after FGA at 275 °C for 3 min. With increasing T_{anneal}, the t_{TiOx}/t_{total} values increased whereas the t_{SiOy}/t_{total} values decreased, indicating that the TiO_x layers of the TiO_x/SiO_y/c-Si heterocontacts became dominant. Furthermore, the amplitude of $\varepsilon_1(E)$ and $\varepsilon_2(E)$ curves of the ALD-TiO_x layer decreased as T_{depo} and T_{anneal} increased due to enhanced diffusion of Ti atoms into SiO_y interlayers at higher T_{depo} and T_{anneal}, which leads to Si incorporated TiO_x become dominant. Therefore, we concluded that the improved τ_{eff} is attributed to adequate formation of mixed oxide consisting of Si, Ti and O atoms. At lower T_{anneal} than 275 °C the diffusion of Ti and O atoms is insufficient, leading to unripe mixed oxide layer. On the other hand, the excessive diffusion of Ti atoms happens at higher T_{anneal} than 275 °C, which results in metal contamination against c-Si surface.

Acknowledgments

This work was supported by the New Energy and Industrial Technology Development Organization (NEDO), MEXT, Grants-in-Aid for Scientific Research on Innovative Areas “Hydrogenomics”, JP18H05514.

References

1) E. Kobayashi, S. De Wolf, J. Levrat, A. Descoeudres, M. Despeisse, F-J. Haug, and C. Ballif, Sol. Energy Mater. Sol. Cells **173**, 43 (2017).
2) L. Korte, E. Conrad, H. Angermann, S. Stangl, and M. Schmidt, Sol. Energy Mater. Sol. Cells **93**, 905 (2009).
3) M. Tanaka, M. Taguchi, T. Matsuyama, T. Sawada, S. Tsuda, S. Nakano, H. Hanafusa, and Y. Kuwano, Jpn. J. Appl. Phys. **31**, 3518 (1992).
4) K. Yoshikawa, W. Yoshida, T. Irie, H. Kawasaki, K. Konishi, H. Ishibashi, T. Asatani, D. Adachi, M. Kanematsu, H. Uzu, and K. Yamamoto, Sol. Energy Mater. Sol. Cells **173**, 37 (2017).
5) M. Taguchi, A. Yano, S. Tohoda, K. Matsuyama, Y. Nakamura, T. Nishiwaki, K. Fujita, and E. Maruyama, IEEE J. Photovolt. **4**, 96 (2014).
6) H. Mehmood, H. Nasser, T. Tauqeer, and R. Turan, Renewable Energy **143**, 359 (2019).
7) H. Mehmood, H. Nasser, E. Özkol, T. Tauqeer, S. Hussain, and R. Turan, Proc. IEEE Int. Conf. Eng. Technnol., 1 (2018).
8) X. Yang, P. Zheng, Q. Bi, and K. Weber, Solar Energy Mater. Sol. Cells **150**, 32 (2016).
9) X. Yang, Q. Bi, H. Ali, K. Davis, W.V. Schoenfeld, and K. Weber, Adv. Mater. **28**, 5891 (2016).
10) B. Liao, B. Hoex, A.G. Aberle, D. Chi, and C.S. Bhatia, Appl. Phys. Lett. **104**, 253903 (2014).
11) B. Liao, B. Hoex, K.D. Shetty, P.K. Basu, and C.S. Bhatia, IEEE J. Photovoltaics **5**, 1062 (2015).
12) G. Sahasrabudhe, S.M. Rupich, J. Jhaveri, A.H. Berg, K.A. Nagamatsu, G. Man, Y.J. Chabal, A. Kahn, S. Wagner, J.C. Sturm, and J. Schwartz, J. Am. Chem. Soc. **137**, 14842 (2015).
13) K.M. Gad, D. Vossing, A. Richter, B. Rayner, L.M. Reindl, S.E. Mohney, and M. Kasemann, IEEE J. Photovoltaics **6**, 649 (2016).
14) M.M. Plakhotnyuk, N. Schuler, E. Shkodin, R.A. Vijayan, S. Masilamani, M. Varadharajaperumal, A. Crovetto, and O. Hansen, Jpn. J. Appl. Phys. **56**, 1 (2017).
15) V. Titova, B. Veith-Wolf, D. Startsev, and J. Schmidt, Energy Procedia **124**, 441 (2017).
16) T. Mochizuki, K. Gotoh, A. Ohta, S. Ogura, Y. Kurokawa, S. Miyazaki, K. Fukutani, and N. Usami, Appl. Phys. Express **11**, 102301 (2018).
17) T. Mochizuki, K. Gotoh, Y. Kurokawa, T. Yamamoto, and N. Usami, Adv. Mater. Interfaces **6**, 1801645 (2018).

18) X. Yang, K. Weber, Z. Hameiri, and S. De Wolf, Prog. Photovolt. Res. Appl. **25**, 896 (2017).
19) K. Gotoh, T. Mochizuki, T. Hojo, Y. Shibayama, Y. Kurokawa, and N. Usami, Curr. Appl. Phys. **21**, 36-42 (2021).
20) Awaji N., Sugita Y., Ohkubo S., Nakanishi T., Takasaki K. and Komiya S., Jpn. J. Appl. Phys. 34, L1013 (1995).
21) Y. Sugita, S. Watanabe, and N. Awaji, Jpn. J. Appl. Phys. **35**, 5437 (1996).
22) J.A. Woollam, B.D. Johs, C.M. Herzinger, J.N. Hilfiker, R.A. Synowicki, and C.L. Bungay, Crit. Rev. Opt. Sci. Technol. **CR72**, 3-28 (1999).
23) B. Johs, J.A. Woollam, C.M. Herzinger, J.N. Hilfiker, R.A. Synowicki, and C.L. Bungay, Crit. Rev. Opt. Sci. Technol. **CR72**, 29-58 (1999).
24) H.G. Tompkins and J.N. Hilfiler, *Spectroscopic Ellipsometry: Practical Application to Thin Film Characterization* (Momentum Press, New York, 2016).
25) K. Gotoh, H. Miura, A. Shimizu, Y. Kurokawa, and N. Usami, Ext. Abstr. Solid State Devices and Materials, 2020, p. 399.
26) A. Cuevas and R.A. Sinton, Prog. Photovolt. Res. Appl. **5**, 79 (1997).
27) R.A. Sinton and A. Cuevas, Appl. Phys. Lett. **69**, 2510 (1996).
28) G.E. Jellison Jr and F.A. Modine, Appl. Phys. Lett. **69**, 2137 (1996).
29) S. Kageyama, M. Akagawa, and H. Fujiwara, Phys. Rev. B **83**, 195205 (2011).
30) C.M. Herzinger, B. Johs, W.A. McGahan, J.A. Woollam, and W. Paulson, J. Appl. Phys. **83**, 3323 (1998).
31) M. Reiners, K. Xu, N. Aslam, A. Devi, R. Waser, and S. Hoffmann-Eifert, Chem. Mater. **25**, 2934 (2013).
32) D. Mardare and P. Hones, Mater. Sci. Eng. **B68**, 42 (1999).
33) S.B. Amor, G. Baud, J.P. Besse, M. Jacquet, Mater. Sci. Eng. **B47**, 110-118 (1997).
34) D. Macdonald and L.J. Geerlings, Appl. Phys. Lett. **85**, 4061 (2004).
35) S.A. McHugo, A.C. Thompson, I. Périchaud, and S. Martinuzzi, Appl. Phys. Lett. **72**, 3482 (1998).
36) A.A. Istratov, T. Buonassisi, R.J. McDonald, A.R. Smith, R. Schindler, J.A. Rand, J.P. Kalejs, and E.R. Weber, J. Appl. Phys. **94**, 6552 (2003).

Figure Captions

Fig. 1. Schematic optical model of the SE analysis. (Color online)

Fig. 2. (a) Effective carrier lifetime of the as-deposited and annealed TiO_x/SiO_y/c-Si heterocontacts as a function of minority carrier density (MCD). The annealing temperature and duration were 275 °C and 3 min, respectively. (b) Effect of annealing temperature on effective carrier lifetime at MCD of 1×10^{15} cm^{-3}. (c) Dependence of effective carrier lifetime at minority carrier density of 1×10^{15} cm^{-3} on deposition temperature. (Color online)

Fig. 3. Amplitude ratio (ψ) and phase difference (Δ) spectra of the TiO_x/SiO_y/c-Si heterocontacts fabricated at deposition temperature of 175 °C (a) before and (b) after annealing at 275 °C for 3 min. The red, green, and dotted lines represent experimental ψ, Δ, and fitting curves, respectively. (Color online)

Fig. 4. (a) total layer thickness of the TiO_x/SiO_y/c-Si heterocontacts (t_{total}), (b) ratio of layer thickness of the ALD-TiO_x layers (t_{TiOx}) to t_{total} and (c) ratio of layer thickness of the SiO_y interlayers (t_{SiOy}) to t_{total} as a function of annealing temperature. (Color online)

Fig. 5. Real and imaginary parts of dielectric functions of the TiO_x layers prepared at T_{depo} = (a) 125, (b) 175, and (c) 225 °C. (Color online)

Fig. 6. Refractive index of the TiO_x layers at a wavelength of 500 nm as function of deposition and annealing temperature. (Color online)

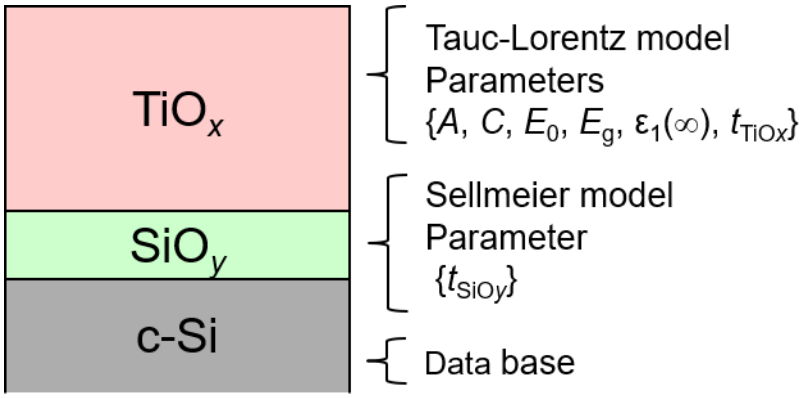
TiO$_x$
SiO$_y$
c-Si
Tauc-Lorentz model
Parameters
{A, C, E_0, E_g, $\varepsilon_1(\infty)$, t_{TiOx}}
Sellmeier model
Parameter
{t_{SiOy}}
Data base

Fig. 1

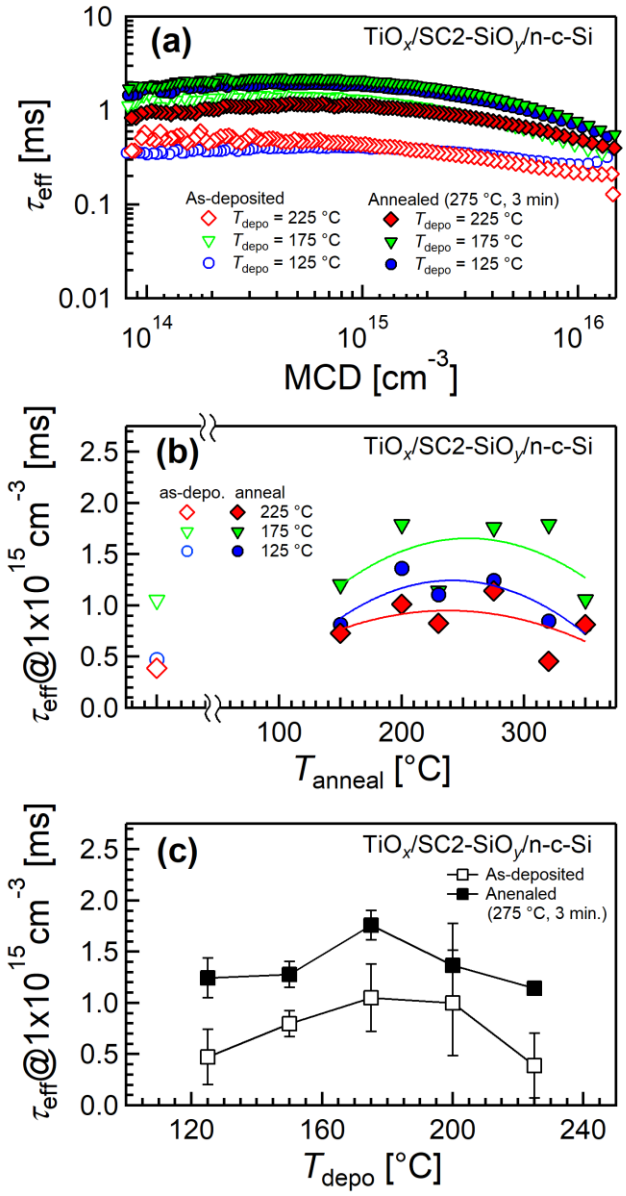
(a)
TiOx/SC2-SiOy/n-c-Si
τeff [ms]
As-deposited
Tdepo = 225 °C
Tdepo = 175 °C
Tdepo = 125 °C
Annealed (275 °C, 3 min)
Tdepo = 225 °C
Tdepo = 175 °C
Tdepo = 125 °C
MCD [cm-3]
(b)
TiOx/SC2-SiOy/n-c-Si
as-depo.
anneal
225 °C
175 °C
125 °C
τeff@1x10^15cm-3 [ms]
Tanneal [°C]
(c)
TiOx/SC2-SiOy/n-c-Si
As-deposited
Anenaled
(275 °C, 3 min.)
τeff@1x10^15cm-3 [ms]
Tdepo [°C]

Fig. 2.

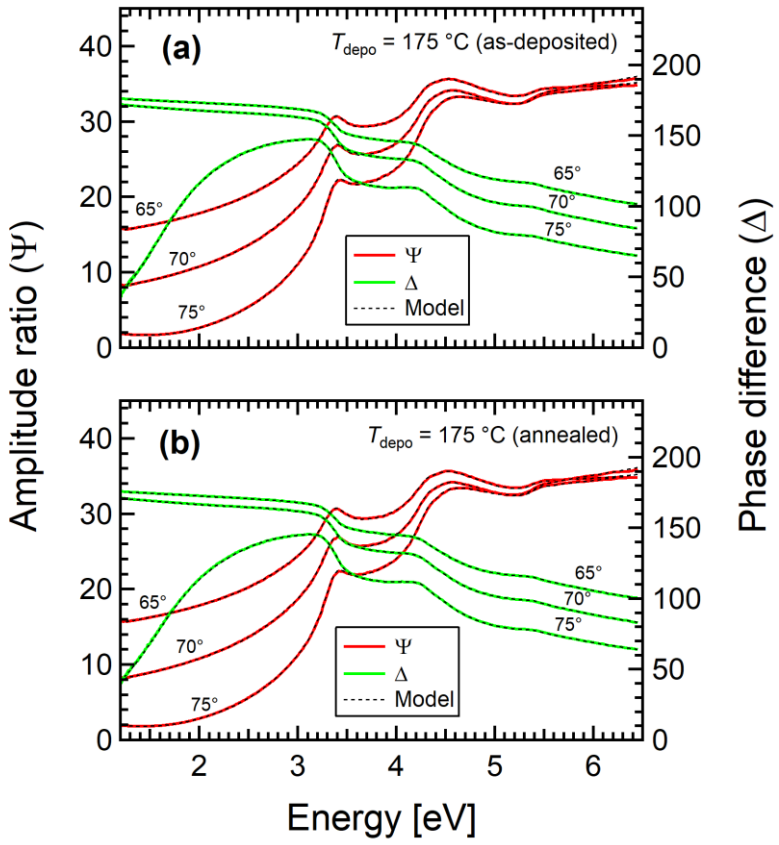
(a)
T_{depo} = 175 °C (as-deposited)
(b)
T_{depo} = 175 °C (annealed)
Ψ
Δ
Model
65°
70°
75°
Amplitude ratio (Ψ)
Phase difference (Δ)
Energy [eV]
0
10
20
30
40
50
100
150
200
2
3
4
5
6

Fig. 3.

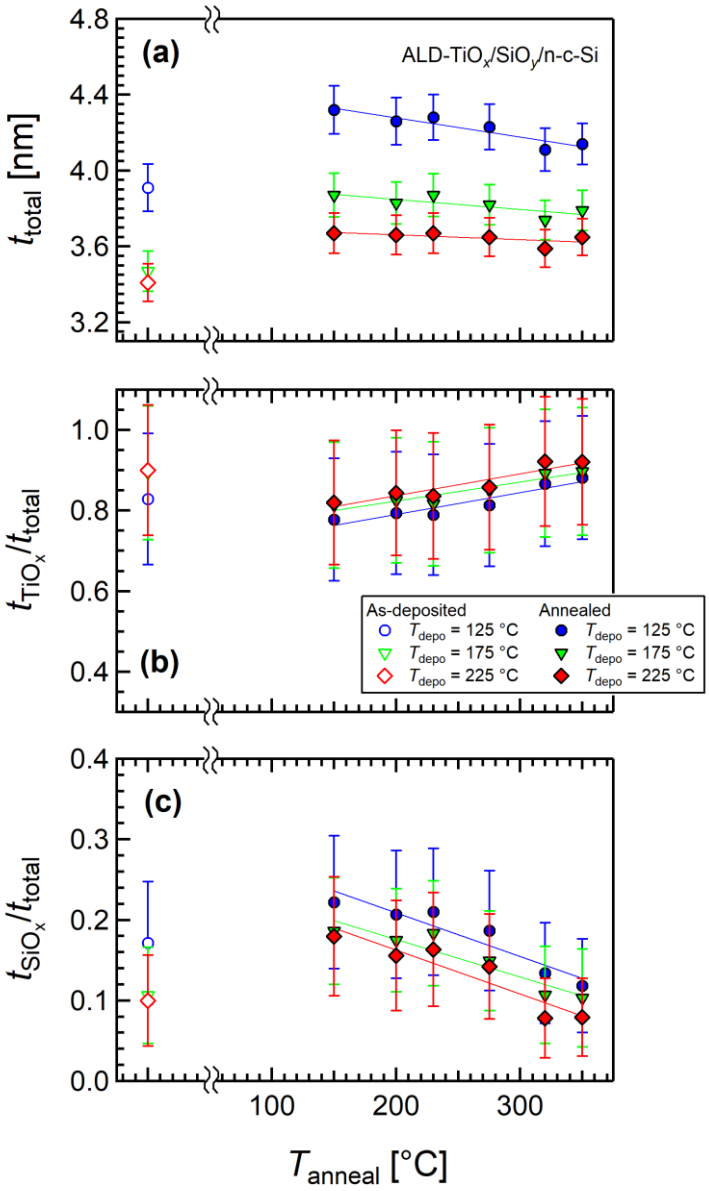
(a)
ALD-TiO$_x$/SiO$_y$/n-c-Si
t_{total} [nm]
4.8
4.4
4.0
3.6
3.2
(b)
t_{TiO_x}/t_{total}
1.0
0.8
0.6
0.4
As-deposited
T_{depo} = 125 °C
T_{depo} = 175 °C
T_{depo} = 225 °C
Annealed
T_{depo} = 125 °C
T_{depo} = 175 °C
T_{depo} = 225 °C
(c)
t_{SiO_x}/t_{total}
0.4
0.3
0.2
0.1
0.0
100
200
300
T_{anneal} [°C]

Fig. 4.

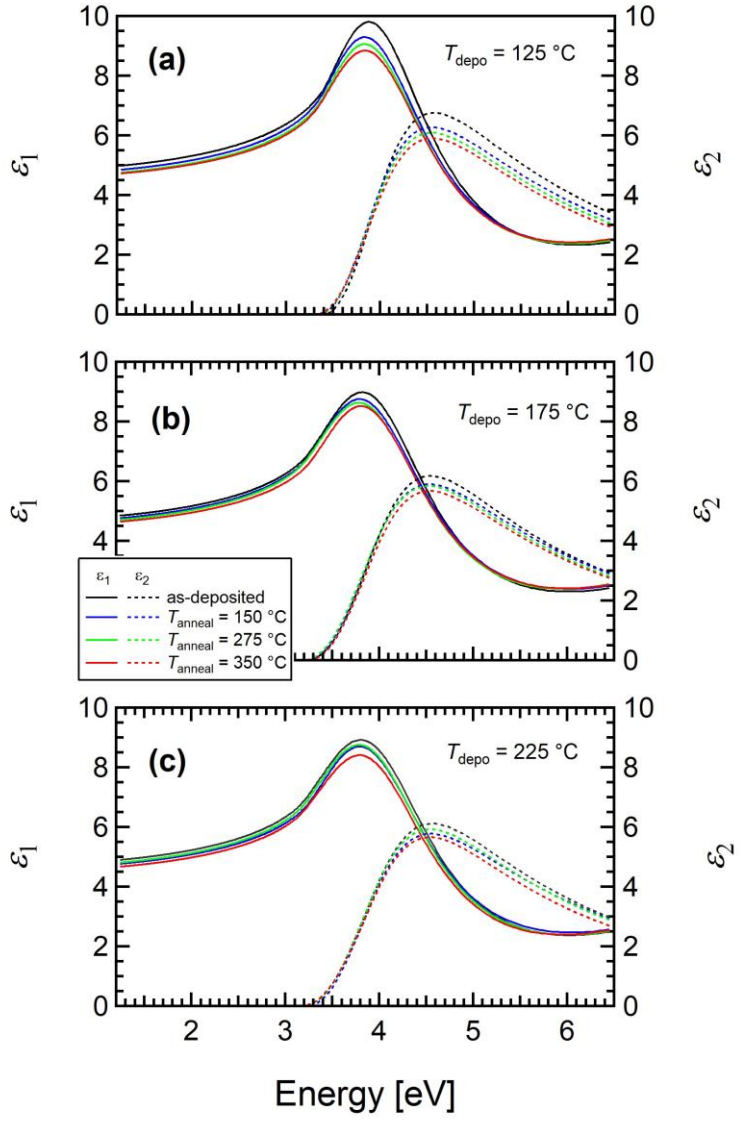
(a)
T_{depo} = 125 °C
(b)
T_{depo} = 175 °C
(c)
T_{depo} = 225 °C
ε_1
ε_2
ε_1 ε_2
as-deposited
T_{anneal} = 150 °C
T_{anneal} = 275 °C
T_{anneal} = 350 °C
Energy [eV]

Fig. 5.

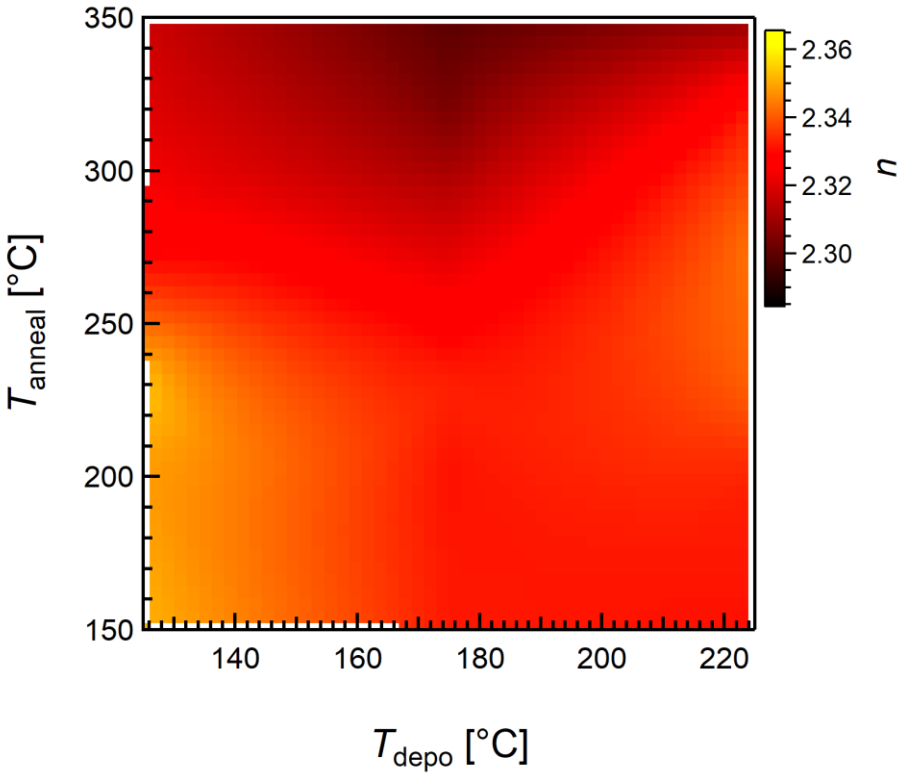
350
300
250
200
150
T_{anneal} [°C]
140
160
180
200
220
T_{depo} [°C]
2.36
2.34
2.32
2.30
n

Fig. 6.